J. Chem. Sci., Vol. 120, No. 6, November 2008, pp. 557–564.

Synthesis and spectroscopic study of high quality alloy $Cd_xZn_{1-x}S$ nanocrystals†

SUPARNA SADHU and AMITAVA PATRA*

Department of Materials Science and Centre for Advanced Materials,
Indian Association for the Cultivation of Science, Kolkata 700 032
e-mail: msap@iacs.res.in

Abstract. In the present study, we report the synthesis of high quality $Cd_xZn_{1-x}S$ nanocrystals alloy at 150°C with changing the composition. The shifting of absorption and emission peak in shorter wavelength is obtained with increasing the mole fraction of zinc. The quantum yield (QY) value decreases with increasing the Cd mole fraction and the values are 0·08, 0·13 and 0·40 for $Cd_{0·62}Zn_{0·38}S$, $Cd_{0·52}Zn_{0·48}S$ and $Cd_{0·31}Zn_{0·69}S$ nanocrystals, respectively after 120 min of reaction. However, the full width at half-maximum (fwhm) values are 45, 34 and 28 nm and the corresponding quantum yield (QY) values are 0·52, 0·17 and 0·13 for 0·5 mM, 1·5 mM and 3 mM of initial S concentrations, respectively. It is interesting to note that the radiative decay time is dominating with increasing the Cd content. Analysis suggests that the decay dynamics depends on the composition of $Cd_xZn_{1-x}S$ nanocrystals.

Keywords. Nanocrystals; $Cd_xZn_{1-x}S$; photoluminescence; time-resolved spectroscopy.

1. Introduction

Semiconductor nanocrystals have attracted much attention in both fundamental research and technological applications, owing to their unique size dependent optical and electronic properties.[1–9] The size dependence of the band gap is the most identified aspect of quantum confinement in semiconductors; the band gap increases as the size of the particles decreases. In alloy nanocrystals, the colour-tuning emission properties are controlled by changing their constituent stoichiometry without changing the particle size.[10–16] Zhong *et al*[11,12] reported ternary alloyed nanocrystals at high temperature (250–330°C). Ying and co-worker demonstrated[8] glutathione capped ZnSe and $Zn_xCd_{1-x}Se$ QDs with tunable optical properties from 360 to 500 nm with high quantum yields of up to 50%. Bailey and Nie[9] reported ternary $CdSe_{1-x}Te_x$ alloy nanocrystals with tunable optical properties. They demonstrated that the composition and internal structure are two important factors which can tune the optical properties without changing the particle size. Only a limited number of studies have been reported for the synthesis of alloy nanocrystals via wet chemical methods.[8,10–12] Therefore, the development of well controlled synthetic methods by controlling compositions remains a challenging problem in materials chemistry. Generally, most of the cases, the used chemicals are extremely toxic, expensive and using relatively high temperature. The synthetic method reported in this paper differs from earlier reports of $Zn_xCd_{1-x}S$ nanoalloys. In the present study, the synthesis temperature is 150°C which is below than reported[11] synthesis temperature (250–330°C).

No detailed report has been found on the time resolved spectroscopic study of $Cd_xZn_{1-x}S$ alloyed nanocrystals with changing the composition, to our knowledge. The detailed understanding of decay dynamics is essential because it dictates the overall efficiency of the materials. Time resolved fluorescence measurement is essential to understand the mechanism of charge carrier relaxation. Furthermore, the radiative and non-radiative decay rates were calculated based on the observed lifetime and fluorescence quantum yield. Of particular interest of our research program is how the photo physics vary with changing the composition, with the hope that such knowledge will enable us to construct efficient nanomaterials for photonic and biophotonic applications.

2. Experimental

2.1 *Materials*

Oleylamine (Aldrich), Dodecylamine (Aldrich), Octylamine (Aldrich), Cadmium acetate (Merck), Zinc

† Dedicated to Prof. C N R Rao on his 75th birthday
*For correspondence

acetate (Merck) and Sulfur powder were used as received. All solvents (*n*-hexane, toluene, methanol and ethanol) were of GR grade and were used without further purification. The spectroscopic grade *n*-hexane was used for optical study.

2.1a *Preparation of ternary alloyed $Cd_xZn_{1-x}S$ nanocrystals:* The synthesis of ternary alloyed $Cd_xZn_{1-x}S$ nanocrystals were based on the reaction of cadmium acetate and zinc acetate with sulfur powder in presence of different amine solvents i.e. oleylamine (C18), dodecylamine (C12) and octylamine (C8). A series of $Cd_xZn_{1-x}S$ samples ($x = 0{\cdot}62$, $0{\cdot}59$, $0{\cdot}31$) were also prepared under the same experimental conditions by varying the initial amount of precursors. All reactions are carried out in oxygen free inert atmosphere. For the preparation of $Cd_{0.52}Zn_{0.48}S$ sample, 0·066 g cadmium acetate, 0·0548 g zinc acetate were added to 5 ml amine (oleylamine or dodecylamine or octylamine) in a two-necked round bottom flask, and the mixture was heated to 150°C under Ar flow for 20 min to form a clear solution. At this temperature, an excess amount of S powder (dissolved in 2·5 ml of amine) was swiftly injected into the hot reaction mixture under gentle stirring. The reaction mixture was kept at the desired growth temperature (150°C). Small volume (~ 0·5 ml) aliquots of sample were taken at different time intervals after the point of injection and were quenched in 5 ml of cold anhydrous toluene (25°C) to terminate the growth of the particles immediately. The resulting alloyed nanocrystals in toluene solution were precipitated out by using ethanol and isolated by centrifugation and decantation. The extensive purification was done prior to characterization.

2.2 *Characterization*

A JEOL-TEM-2010 transmission electron microscope (operating voltage at 200 kV) was used to analyse the size, size distribution and structure of the resulting nanocrystals. Samples for TEM were prepared by making a clear solution of samples in cyclohexane and placing a drop of the solution on a carbon coated copper grid. The crystalline phases of the nanoparticles were identified by X-ray diffraction (XRD) using a Siemens model D 500, powder X-ray diffractometer using a CuKα source (1·5418 Å radiation). The compositions of the alloyed nanocrystals were determined by means of Shimadzu Atomic Absorption Spectrophotometer AA-6300, equipped with a lamp for Cd and Zn at wavelengths 228·8 and 213·9 nm, respectively. Approximately 1 mg of the nanocrystals powder was digested in concentrated hydrochloric acid and then an aqueous solution was prepared using Mili-Q water for AAS measurement.

Absorption and photoluminescence (PL) spectra of $Cd_xZn_{1-x}S$ QD samples in cyclohexane solution were obtained at room temperature with a Shimadzu UV-2450 UV-Vis spectrometer and a Horiba Jobin Yvon FluoroMax-P fluorescence spectrometer, respectively. Photoluminescence quantum yields (QY) were obtained by comparison with standard dye (Coumarine 440 in methanol), using the standard method. For the time correlated single photon counting (TCSPC) measurements, the samples were excited at 375 nm using a picosecond diode laser in an IBH Fluorocube apparatus. The pulse duration is about 200 ps. The repetition rate is 500 KHz. The fluorescence decays were collected at a Hamamatsu MCP photomultiplier (C487802). The fluorescence decays were analysed using IBH DAS6 software.

3. Results and discussion

Figure 1 represents the XRD pattern of pure ZnS, pure CdS and $Cd_xZn_{1-x}S$ nanocrystals alloy prepared under different conditions. It clearly shows a zinc-blend cubic structure of pure CdS, ZnS and the ternary alloyed nanocrystals over all compositions and exhibit three prominent peaks which are indexed (111), (220), and (311) planes. It is seen that the

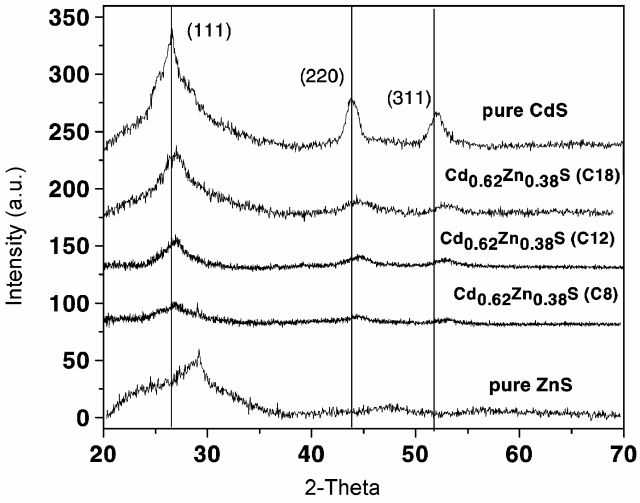

Figure 1. Powder XRD patterns of the CdS, ZnS and $Cd_{0.62}Zn_{0.38}S$ nanocrystals prepared by different amines. The line corresponds to bulk cubic CdS.

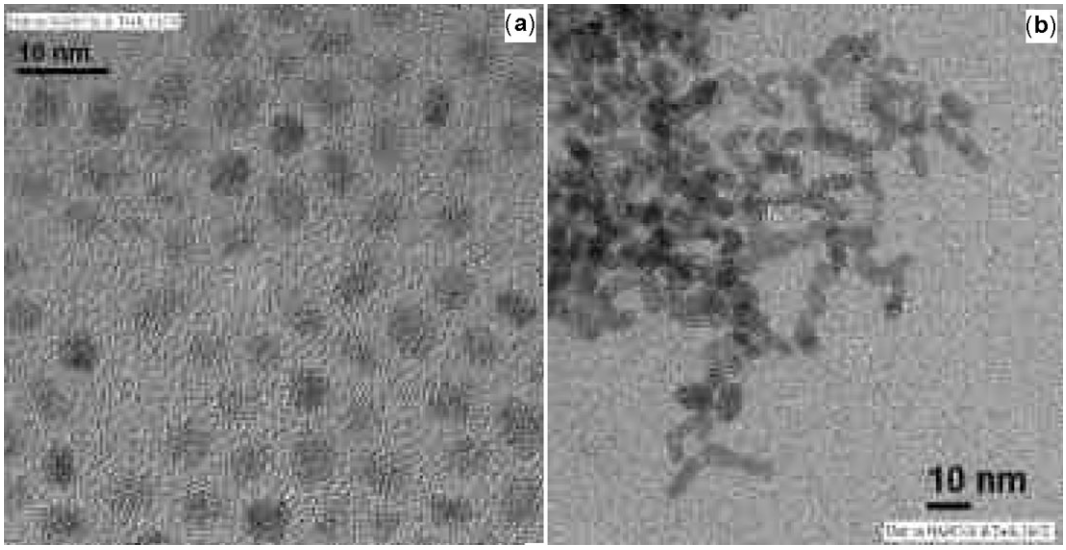

Figure 2. HR-TEM images of $Cd_{0.62}Zn_{0.38}S$ nanocrystals prepared by oleylamine (C18) (**a**) and octylamine (C8) (**b**) at 150°C.

diffraction peaks gradually shift toward larger angles as the Zn content increases.[11] The continuous peak shifting of the mono-dispersed nanocrystals may also rule out phase separation or separated nucleation of either CdS or ZnS nanocrystals. The broad diffraction peaks also imply very small particle size.

Figure 2 shows the HR-TEM images of the as-prepared $Cd_xZn_{1-x}S$ nanocrystals without any size selection after 2 h growth under the above mentioned synthesis conditions, which reveal nanocrystals with well-resolved lattice fringes, demonstrating the highly crystalline nature of the nanocrystals. Nearly mono-disperse particles are observed in all cases. It is seen from figure 2a that $Cd_{0.62}Zn_{0.38}S$ nanocrystals are uniform spherical shape in presence of oleylamine (C18). The average diameter of particle is 4·2 nm. However, the rod shape nanocrystal appears in presence of octylamine (C8) which is shown in figure 2b. The average diameter of the rod is 3·5 nm and average length is 8·2 nm. It reveals that the chain length of amine plays a key role on changing the shape of particle. Further investigation is needed to understand the mechanism.

It is already reported[11] that cadmium is considerably more reactive than zinc toward sulfur and the growth rate of CdS is larger than that for ZnS. In this study, all reagents are added into a single pot by varying the initial Cd : Zn molar ratio. The amount of the injected S is either in large excess or in equal supply relative to the total mole amount of cadmium and zinc. At the very initial stage of the reaction, the CdS seeds formation occurs rapidly and then ZnS deposition starts onto it. The alloyed nanocrystals with composition fluctuations can grow up at 150°C where the internal atom diffusion can convert these into a homogeneous alloy.[11] Particle growth will stop only after the consumption of all free S and yielding homogeneous alloyed QDs. This alloying process is clearly demonstrated by temporal evolution of the absorption and the photoluminescence spectra during rapid particle nucleation and growth in figure 3. It is interesting to note that the absorption onset was 404 nm at 1 min and it was shifted to 415 nm after 60 min which is then fixed even after 6 h (figure 3a). In the PL spectra, the initial broad emission peak gradually turns into a narrow one and the emission peak at 423 nm after 5 min of reaction is shifted to 429 nm after 1 h then become fixed which corresponds that the initial gradient alloyed QDs converted into the homogeneous alloy after a certain reaction time. The time required to form homogeneous alloy also depends on the initial concentration of S. When a large excess of S precursor is used, the surface of initially formed CdS seeds is S-rich. This is helpful for the deposition of ZnS, which can form alloy simultaneously with CdS via the internal self-diffusion.

Figure 4 shows the photoluminescence spectra of pure CdS, pure ZnS and $Cd_{0.62}Zn_{0.38}S$ nanocrystals prepared by oleylamine, dodecylamine and octylamine, respectively. The PL peaks are 502 nm, 404 nm, 454 nm, 456 nm and 457 nm for pure CdS,

ZnS and $Cd_{0.62}Zn_{0.38}S$ nanocrystal prepared by oleylamine, dodecylamine and octylamine, respectively. Figure 5 shows the plot of Cd mole fraction vs PL peak where the PL peaks are at 502, 454, 437, 425 and 403 nm for pure CdS, $Cd_{0.62}Zn_{0.38}S$, $Cd_{0.52}Zn_{0.48}S$, $Cd_{0.31}Zn_{0.69}S$ and pure ZnS nanocrystals, respectively, indicating the shifting of emission peak in shorter wavelength with increasing the mole fraction of zinc. It shows a nearly linear relationship of PL peaks with the Cd mole fraction, which confirms the formation of homogeneous alloy structure. The obtained systematic composition-controlled shift of the absorption onset and the emission maxima to shorter wavelength can be explainable by considering the formation of $Cd_xZn_{1-x}S$ nanocrystals via intermixing of wider band gap ZnS (3·7 eV) with narrower band gap CdS (2·5 eV) nanocrystals, rather than forming separate CdS and ZnS nanoparticles or core-shell structure.[11] It is interesting to note that the quantum yield (QY) value decreases with increasing the Cd mole fraction and the values are 0·08, 0·13 and 0·40 for $Cd_{0.62}Zn_{0.38}S$, $Cd_{0.52}Zn_{0.48}S$ and $Cd_{0.31}Zn_{0.69}S$ nanocrystals, respectively after 120 min of reaction. The QY values are 0·08, 0·04 and 0·01 for $Cd_{0.62}Zn_{0.38}S$ nanocrystal prepared by oleylamine, dodecylamine

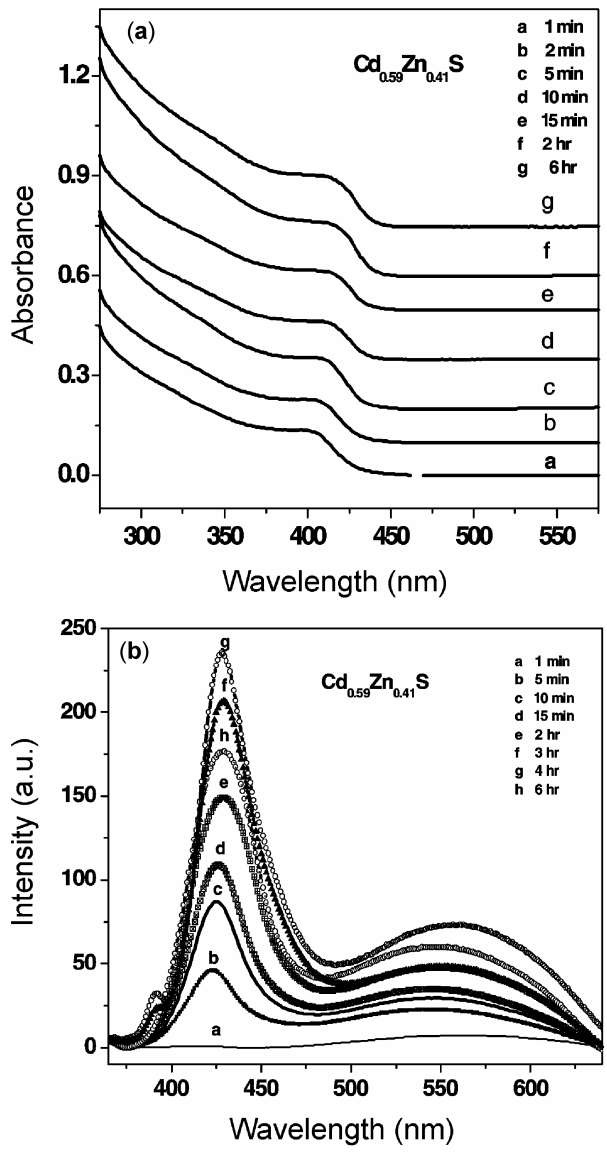

Figure 3. Temporal evolutions of absorption (**a**) and photoluminescence spectra (**b**) of $Cd_{0.59}Zn_{0.41}S$ nanocrystals during their growth at 150°C temperature.

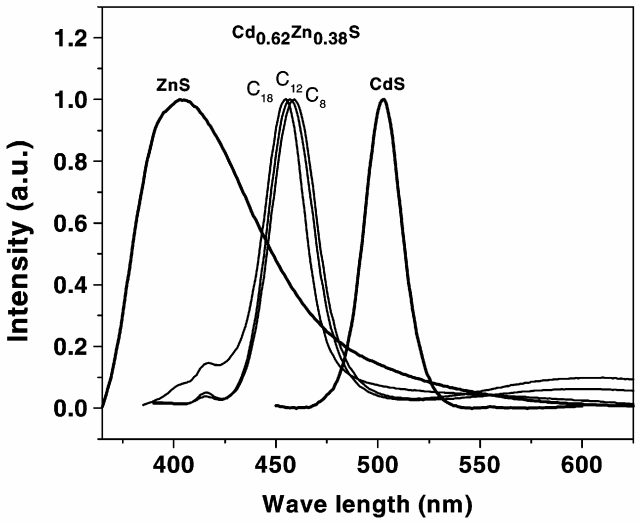

Figure 4. Photoluminescence spectra of pure CdS, ZnS and $Cd_{0.62}Zn_{0.38}S$ nanocrystals prepared by different amines.

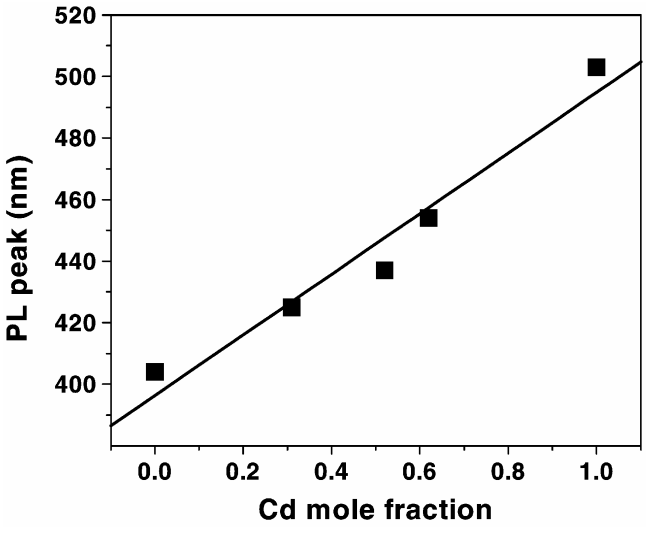

Figure 5. A plot of Cd mole fraction vs PL peak of pure CdS, ZnS, $Cd_{0.62}Zn_{0.38}S$, $Cd_{0.52}Zn_{0.48}S$ and $Cd_{0.31}Zn_{0.69}S$ nanocrystals.

and octylamine, respectively. Coordinating probability increases with increasing the chain length due to inductive effect. Therefore, oleylamine shows better capping or coordinating agent than octylamine and dodecylamine. This may be the reason to produce higher quantum yield of oleyamine capped nanoparticle. Peng *et al*[17] also reported that the minimum of the PL fwhm gradually increases while the initial Cd : Se ratio of the precursors increased from 1 : 10 to 2 : 1. Meijerink *et al* also investigated the temporal evolution of photoluminescence quantum yields of colloidal CdSe nanocrystals during their growth at different temperatures.[18] In general, a low PL QY is considered as a result of the surface states located in the band gap of the nanocrystals, which act as trapping states for the photo generated charges. CdS seeds start nucleation and growth upon injection of S solution and the ZnS deposited relatively in slower rate on the surfaces of CdS nanocrystals. At the initial stage of the alloy formation, there is a generation of defects on the surface of the nanocrystals by cation exchange and gets low PL QY. With further progress of reaction, the internal atom diffusion helps the formation of homogeneous alloy and the gradual increase in QY is due to the removal of surface defects from the alloyed nanocrystals.

The influence of the initial molar concentration of S on the optical properties of $Cd_xZn_{1-x}S$ alloyed nanocrystals investigated for three different values (0·5 mM, 1·5 mM and 3 mM), while keeping the other reaction parameters same. Figure 6 shows the absorption and photoluminescence spectra of $Cd_xZn_{1-x}S$ nanocrystals with different molar concentration of S. In the absorption spectra, the first excitonic absorption peaks are at 410, 416 and 427 nm and the corresponding emission peaks are at 426, 431 and 437 nm for $Cd_xZn_{1-x}S$ nanocrystals with S molar concentrations are 0·5 mM, 1·5 mM and 3 mM, respectively, indicating the shifting of PL peak in longer wavelength with increasing the concentration of S. The full width at half-maximum (fwhm) values are 45, 34 and 28 nm and the corresponding quantum yield (QY) values are 0·52, 0·17 and 0·13 for S concentrations 0·5 mM, 1·5 mM and 3 mM, respectively. The presence of broad PL band emission around 550 nm, particularly for S concentration 0·5 mM, indicates the presence of surface states.[19] These surface states have been attributed to S-unsaturated bonds and serve as carrier traps.[19] In the present study, amines are used as capping agent which forms strong complex with Cd and Zn via nitrogen lone pair and since nitrogen is strong electronegative, so it does not introduce hole traps.[20] The maximum quantum efficiency at 0·5 mM of S concentration indicates the perfect passivation effect of $Cd_xZn_{1-x}S$ nanocrystals by oleylamine. Relatively lower quantum efficiency is observed at higher concentration (1·5 mM and 3 mM) of S because excess S^{2-} also form surface states from S-unsaturated bonds which will serve as carrier traps. Therefore, optimum S^{2-} content is required for making efficient nanomaterials.

To understand the decay dynamics of these nanoalloys, we measured decay time using pulsed excitation and time-correlated single-photon counting (TCSPC) at the maxima fluorescence. Figure 7

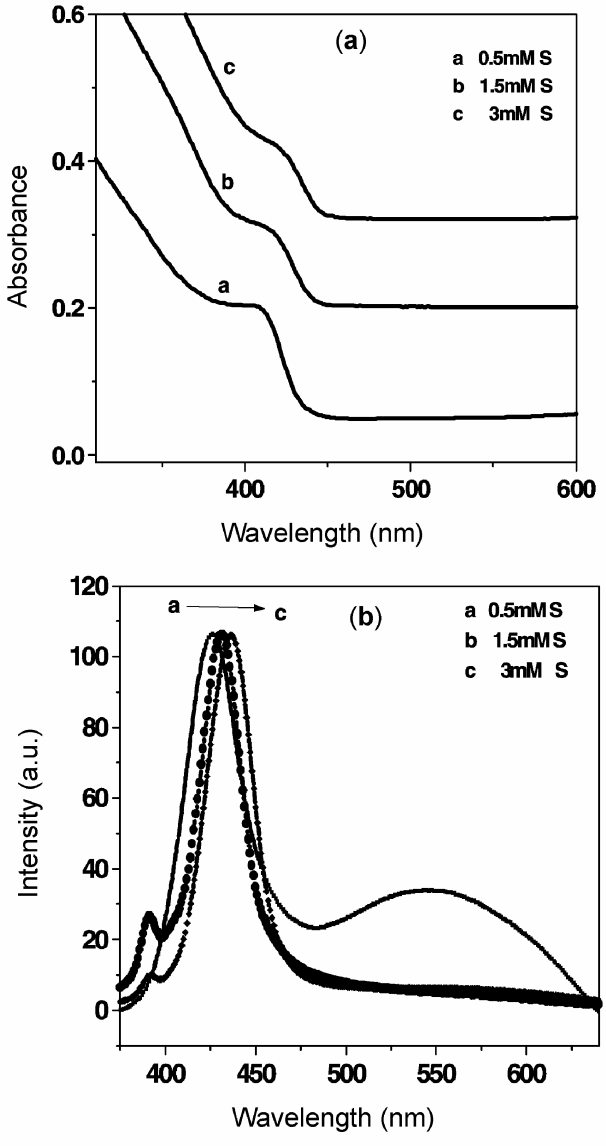

Figure 6. Absorption (**a**) and photoluminescence (**b**) spectra of $Cd_xZn_{1-x}S$ nanocrystals with different molar concentrations of S precursor.

Table 1. Flourescence decay of $Cd_xZn_{1-x}S$ nanoalloy with varying composition.

Sample	χ^2	τ_1 (ns) (α_1)	τ_3 (ns) (α_3)	τ_3 (ps) (α_3)	$\langle T \rangle$ (ns)	τ_r (ns)	τ_{nr} (ns)
$Cd_{0.31}Zn_{0.69}S$ (C_{18})	1·17	0·77 (36.45)	4·11 (31·8)	104·7 (31·75)	3·5	9·77	5·33
$Cd_{0.52}Zn_{0.48}S$ (C_{18})	1·02	1·36 (38·07)	7·91 (47·52)	279 (14·42)	7·05	54·21	8·1
$Cd_{0.62}Zn_{0.38}S$ (C_{18})	1·18	1·66 (35·06)	8·94 (51·08)	306 (13·86)	8·05	100·66	8·75
$Cd_{0.62}Zn_{0.38}S$ (C_{12})	1·12	2·24 (29·53)	14·17 (58·78)	356 (11·69)	13·23	286·39	13·87
$Cd_{0.62}Zn_{0.38}S$ (C_8)	1·08	2·38 (24·03)	15·92 (67·96)	361 (8·01)	15·20	993·6	15·44

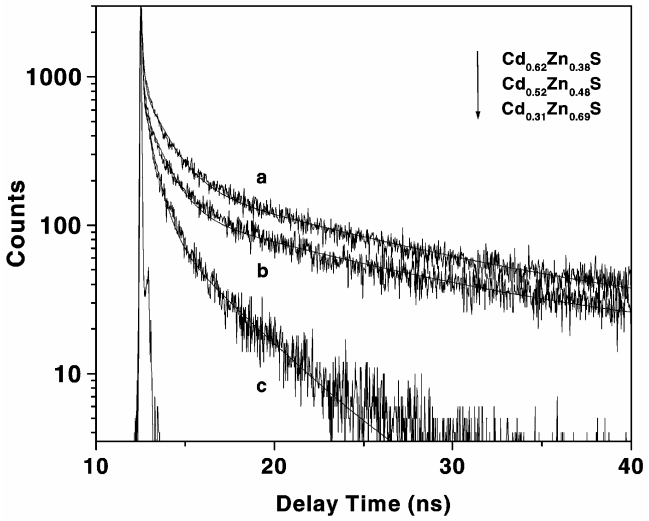

Figure 7. Photoluminescence decay profiles of (**a**) $Cd_{0.62}Zn_{0.38}S$, (**b**) $Cd_{0.52}Zn_{0.48}S$ and (**c**) $Cd_{0.31}Zn_{0.69}S$ nanocrystals at the PL emission peak.

shows the photoluminescence decay curves of different composition of $Cd_xZn_{1-x}S$ alloyed nanocrystals. The PL decay profiles are well described by three-exponential function, $I(t) = A_1\exp(-t/\tau_1) + A_2\exp(-t/\tau_2) + A_3\exp(-t/\tau_3)$. The photoluminescence decay of $Cd_{0.31}Zn_{0.69}S$ nanocrystals is tri-exponential with decay components of (τ_1) 0·77 ns (36·45%), (τ_2) 4·11 ns (31·8%) and (τ_3) 104·7 ps (31·75%) and average decay time is 3·5 ns (table 1). The photoluminescence decay of $Cd_{0.52}Zn_{0.48}S$ nanocrystals is tri-exponential with decay components of (τ_1) 1·36 ns (38·07%), (τ_2) 7·91 ns (47·52%) and (τ_3) 279 ps (14·4%) and average decay time is 7·05 ns (table 1). The photoluminescence decay of $Cd_{0.62}Zn_{0.38}S$ nanocrystals is tri-exponential with decay components of (τ_1) 1·66 ns (35·06%), (τ_2) 8·94 ns (51·08%) and (τ_3) 306 ps (13·86%) and average decay time is 8·05 ns (table 1). A variety of relaxation processes that may occur on a wide range of time scales has been reported.[21–27] The most important non-radiative pathway is surface related defects.[21] Kloepfer *et al*[22] already reported multi-exponential decay in CdSe nanocrystals. There is still some debate on the possible mechanisms of deactivated for photoexcited quantum dot nanocrystals. Generally, the photoluminescence originates either from band edge or recombination of surface states energy levels. Surface defects give rise to trap states that lie within the band gap and complicate the dynamics. Electron promotes to conduction band after excitation. Subsequent relaxation to the bottom of the conduction band is rapid. The exciton emission arises from radiative relaxation of these electrons to the ground state and likely contributes to the fastest decay. These conduction electrons may be localized in shallow trap states and from there, these electrons may be repopulated the conduction band or thermalize to deep trap. The lifetime is extended in the former case and the latter contributes to non-radiative mechanisms that lower the overall quantum efficiency.[22] A combination of all these processes gives raise multi-exponential emission dynamics that occurs over a nanosecond time scale and is observed in this experiment. In our study, we recorded the time resolved spectra at the PL peak, which has been attributed to recombination from band edge (1s state). Therefore, we believe that fast process is due to trapping of carriers in surface state, which may be a process much faster than the *e–h* recombination process.[26] The slower process is related to the *e–h* recombination process, which dominates after all the surface defects states have been saturated. The relative contributions of the time constants vary with changing composition, indicating that the trapping processes are different for different compositions. The systematic increase in overall decay times with increasing the Cd content was observed. In the case of $Cd_xZn_{1-x}S$ nanocrystals, the lattice mismatch between ZnS (0·54 nm) and CdS (0·58 nm) would cause the surface trapping. Such traps are energetically located in between the valence and conduction band edge. Recombination of charge carriers in nanoparticles, involving shallow carrier traps which will show delayed fluorescence but longer fluores-

cence lifetimes. In the present study, the lifetime increases with increasing the Cd content, indicating more energy traps are formed. The radiative (τ_r) and non-radiative (τ_{nr}) lifetimes are calculated from the observed emission lifetimes (τ_{ob}) and the fluorescence quantum yield (ϕ_{fl}) using the following equations.[21]

$$\phi_{fl} = \tau_{ob}/\tau_r \quad (1)$$

$$1/\tau_{ob} = 1/\tau_r + 1/\tau_{nr}. \quad (2)$$

It is interesting to note that the radiative lifetime increases from 9·7 ns to 100·6 ns with increasing the Cd content from 0·31 to 0·62 (table 1). Bawendi *et al*[28] already reported that the radiative rate is dominant for decrease in lifetime with increase in PL intensity and quantum yield. In the present study, we observed the systematic decrease in emission intensity, quantum yield and increase in decay times with increasing the Cd content, indicating the radiative rate is dominant.

Figure 8 shows the decay curves of $Cd_{0·62}Zn_{0·38}S$ nanocrystals prepared by oleylamine, dodecylamine and octylamine, respectively. It is found that the fluorescence decay time increases with decreasing the chain length of amine. In dodecylamine (C12), the photoluminescence decay of $Cd_{0·62}Zn_{0·38}S$ nanocrystals is tri-exponential with decay components of (τ_1) 2·24 ns (29·53%), (τ_2) 14·17 ns (58·78%) and (τ_3) 356 ps (11·69%) and average decay time is 13·23 ns (table 1). However, the average decay time is 15·20 ns for $Cd_{0·62}Zn_{0·38}S$ (table 1) in presence of octylamine (C8). It is seen that overall decay time increases with decreasing the alkyl chain length i.e. C18 to C8. Results suggest that surface modification by different ligands can control the decay dynamics of the QD's.

Figure 9 shows the decay curves of $Cd_{0·52}Zn_{0·48}S$ and $Cd_{0·59}Zn_{0·41}S$ for 3 and 0·5 mM concentration of S. It is found that the fluorescence lifetime increases with decreasing the S content. The photoluminescence decay of $Cd_{0·59}Zn_{0·41}S$ nanocrystals is tri-exponential with decay components of (τ_1) 754 ps (5·9%), (τ_2) 4·5 ns (11·1%) and (τ_3) 41 ns (82·9%) for 120 min reaction time and average decay time is 40·4 ns. However, the average decay time is 12·7 ns for $Cd_{0·52}Zn_{0·48}S$. The calculated non-radiative lifetimes are 18·1 ns and 132·9 ns for 3 and 0·5 mM concentration of S. It is seen that the fluorescence lifetime, quantum yield and emission intensity increase with decreasing the S content, indicating that the non-radiative rate is dominant. Therefore, we may say that the carrier trap increases with decreasing the S content and giving rise to slower decays and longer fluorescence lifetimes. Analysis suggests that the radiative and non-radiative relaxation rate depends on the composition of the nanoalloys.

4. Conclusion

In summary, we reported the relatively low temperature (150°C) synthesis of $Cd_xZn_{1-x}S$ alloyed nanocrys-

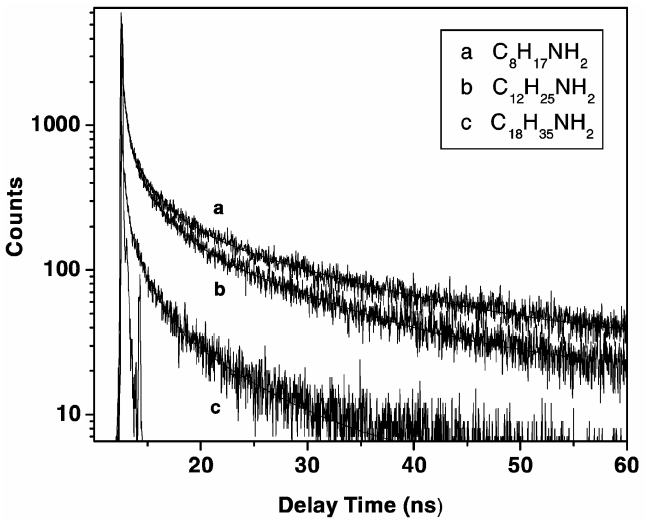

Figure 8. Photoluminescence decay profiles of $Cd_{0·62}Zn_{0·38}S$ nanocrystals prepared by different amines.

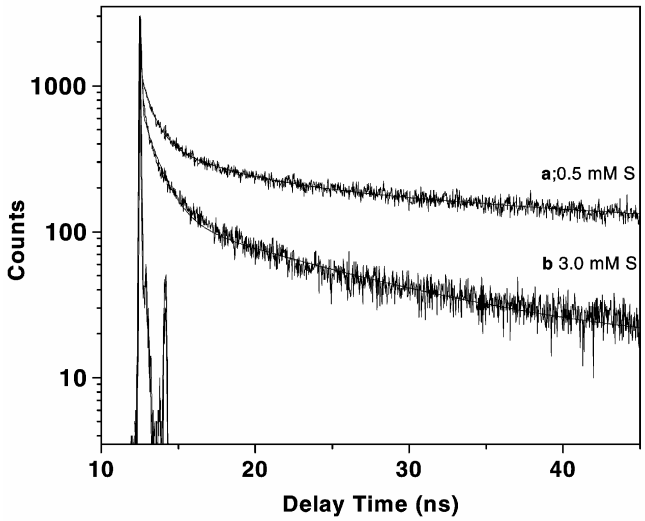

Figure 9. Photoluminescence decay profiles of $Cd_xZn_{1-x}S$ nanocrystals with different molar concentrations of S precursor (**a**) 0·5 mM and (**b**) 3 mM.

tals having PL quantum yields of 23–52% with highly narrow luminescence spectral width of 22–38 nm and study their photophysical properties by steady state and time resolved spectroscopy. Nearly mono-disperse particles are observed for $Cd_{0.62}Zn_{0.38}S$, $Cd_{0.52}Zn_{0.48}S$, $Cd_{0.31}Zn_{0.69}S$ and $Cd_{0.59}Zn_{0.41}S$ nanocrystals, respectively. The full width at half-maximum (fwhm) values of photoluminescence spectrum are 45, 34 and 28 nm and the corresponding quantum yield (QY) values are 0·52, 0·17 and 0·13 for S concentrations 0·5 mM, 1·5 mM and 3 mM, respectively. In the present case, we have also observed that the systematic decrease in emission intensity, quantum yield and increase in decay times with increasing the Cd content, indicating the radiative rate is dominant. The carrier trap increases with decreasing the S content and giving rise to slower decays and longer fluorescence lifetime.

Acknowledgements

The Department of Science and Technology (DST) for financial support and 'Ramanujan Fellowship' are gratefully acknowledged. SS thanks Council of Scientific and Industrial Research (CSIR) for awarding fellowship.

References

1. Brus L E 1984 *J. Chem. Phys.* **80** 4403
2. Alivisatos A P 1996 *Science* **271** 933
3. Ghosh S, Biswas K and Rao C N R 2007 *J. Mater. Chem.* **17** 2412
4. Biswas K and Rao C N R 2007 *Chem-Euro. J.* **13** 6123
5. Sadhu S, Sen T and Patra A 2008 *J. Nanosci. and Nanotech.* **8** 1238
6. Chowdhury P S and Patra A 2006 *Phys. Chem. Chem. Phys.* **8** 1329
7. Talapin D V, Rogach A L, Kornowski A, Hasse M and Weller H 2001 *Nano Lett.* **1** 207
8. Zheng Y G, Yang Z and Ying J Y 2007 *Adv. Mater.* **19** 1475
9. Bailey R E and Nie S 2003 *J. Am. Chem. Soc.* **125** 7100
10. Kim S W, Sujith S and Lee B Y 2006 *Chem. Commun.* 4811
11. Zhong X H, Han M Y, Dong Z L, White T J and Knoll W 2003 *J. Am. Chem. Soc.* **125** 8589
12. Zhong X H, Feng Y, Knoll W and Han M Y 2003 *J. Am. Chem. Soc.* **125** 13559
13. Wang W, Germanenko I and El-Shell M S 2002 *Chem. Mater.* **14** 3028
14. Zhong X, Liu S, Zhang Z, Li L, Wei Z and Knoll W 2004 *J. Mater. Chem.* **14** 2790
15. Huang J, Lianos P, Yang Y and Shen J 1998 *Langmuir* **14** 4342
16. Chen D and Gao L 2005 *Solid State Commun.* **133** 145
17. Qu L and Peng X 2002 *J. Am. Chem. Soc.* **124** 2049
18. Donegá C M, Hickey S G, Wuister S F, Vanmaekelbergh D and Meijerink A 2003 *J. Phys. Chem.* **B107** 489
19. Kortan, A R, Hull R, Opila R L, Bawendi M G, Steigerwald M L, Carroll P J and Brus L E 1990 *J. Am. Chem. Soc.* **112** 1327
20. Sharma H, Sharma S N, Singh G and Shivaprasad S M 2006 *Physics* **E31** 180
21. Wu F, Zhang J Z, Kho R and Mehra R K 2000 *Chem. Phys. Lett.* **330** 237
22. Kloepfer J A, Bradforth S E and Nadeau J L 2005 *J. Phys. Chem.* **B109** 9996
23. Creti A, Anni M, Rossi M Z, Lanzani G, Leo G, Sala F D, Manna L and Lomascolo M 2005 *Phys. Rev.* **B72** 125346
24. Guyot-Sionnest P, Shim M, Matranga C and Hines M 1991 *Phys. Rev.* **B60** R2181
25. Klimov V I 2000 *J. Phys. Chem.* **B104** 6112
26. Sadhu S, Chowdhury P S and Patra A 2008 *J. Lumin.* **128** 1235
27. Chowdhury P S, Ghosh P and Patra A 2007 *J. Lumin.* **124** 327
28. Fisher B R, Eisler H J, Stott N E and Bawendi M G 2004 *J. Phys. Chem.* **B108** 143